

Accurate Pointing Determination of Space Targets under the Stars Background

Zhichao Guan ¹, Chongyuan Hou ¹, Xing Zhong ², Yonghua Jiang ³, Guo Zhang ¹, Jing Gong ⁴

¹ State Key Laboratory of Information Engineering in Surveying, Mapping and Remote Sensing (LIESMARS), Wuhan University, Wuhan 430079, China - guanzhichao@whu.edu.cn, houzenan@163.com, guozhang@whu.edu.cn

² Chang Guang Satellite Technology CO, LTD, Changchun 130033, China - ciomper@163.com

³ School of Remote Sensing and Information Engineering, Wuhan University, Wuhan 430079, China - jiangyh@whu.edu.cn

⁴ Wuhan Xuanjing Technology CO, LTD, Wuhan 430223, China - m201472419@alumni.hust.edu.cn

Keywords: Space targets, Camera calibration, Pointing determination, Jilin-1, Identify stars.

Abstract

This study proposes a method for determining the direction of space targets using existing satellite constellations. Usually, when optical satellites point towards deep space for imaging, stars inevitably appear in the image. This study conducts all targets extraction, star identification, camera calibration. Ultimately obtaining high-precision space targets longitude and latitude information. One of the Jilin-1 GF06A series satellite was used to conduct observation experiments on space targets of this study. Each scene has an exposure time of 10 seconds, and a total of 90 seconds of observation data was obtained. This study analysed the results of star extraction and the identification result which indicate that GF06A can capture a maximum magnitude of 15.6. After using the extraction star coordinate information for calibration, the interior accuracy of camera was better than 0.48 arcseconds. Then, the precise longitude and latitude information of 5 space targets were obtained. Finally, cataloguing information of these stars is provided, which is beneficial for determining the orbit of the target in the future.

1 Introduction

With the increasing number of objects such as artificial satellites, rocket bodies and their debris orbit the Earth, space target monitoring has become an important task in the aerospace field. The risk of spacecraft damage caused by space debris impacts is the third largest risk, second only to risks related to launch and deployment phases (Lupo et al., 2018). At present, space targets are mainly achieved through ground-based observation, including target catalogue, pointing determination, and orbit determination. Traditionally, there are two methods for ground observation: optical and radar (Liu et al., 2022). Ground based radar observation is not affected by light and is not limited by instrument's weight and size. The larger the radar antenna and power, the higher the detection accuracy of the target and the farther the detection distance. However, the signal loss of the target is proportional to the fourth power of the distance, and ground radar monitoring is usually limited to low Earth orbit (LEO) targets. The detection method of ground-based optical, where the brightness attenuation of the space target is proportional to the square of the distance, can be used to detect targets in higher orbits. The European Space Agency (ESA) has established the Schmidt telescope to detect objects up to 15cm in size in geosynchronous orbit (GEO). The simulation results show that the estimation accuracy of satellite position is better than 5 arcseconds (Samadzadegan et al., 2013). However, due to factors such as atmospheric environment, sunlight, and weather, the size and accuracy of space targets monitored by ground-based optical monitoring are limited. In addition, due to the latitude limitation of a single foundation system, the sustained observation ability of certain targets is restricted for ground based observation (Gruntman et al., 2014).

In recent years, the gradually established LEO satellite constellations can be used to observe and measure space targets, effectively avoiding the above drawbacks. For instance, the U.S.

DoD (Department of defence) is planned to establish a constellation for tracking space objects, which is called the SBSS (Space-Based Surveillance System). The Canada has been also designed for the monitoring of space debris from LEO as part of the Canadian space surveillance system (CSSS) (Lupo et al., 2018). As shown in Figure 1, this study mainly uses Jilin-1 optical satellite constellations in LEO to observe space targets in medium to high orbits, such as satellites in high elliptical orbits (HEO) and GEO satellites.

During the process of imaging with an optical camera aimed at deep space, stars inevitably appear in the image and are confused with the target information. The recognition and extraction of stars can not only eliminate the interference of stars, but also can be used as stars control points (SCPs) to improve the pointing accuracy and eliminate interior distortions of the camera (Guan et al., 2023). Thereby, the pointing determination accuracy of the space target could be further improving.

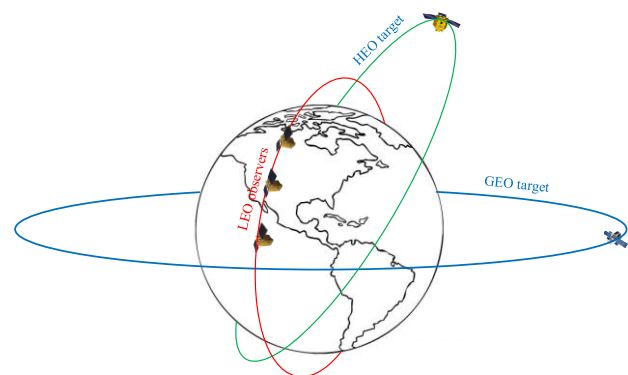


Figure 1. The LEO constellations observe HEO and GEO target.

2 Method

This study will achieve high precision pointing determination of space target through four steps as Figure 2 shown. First, the data is pre-processed to remove background noise from the image, and all the potential targets are extracted. Second, identify stars within the camera's field of view based on the geometric imaging model and existing star catalogue data. The third step has two optional options, one is to calibrate the camera based on the extracted stars. Another step is to remove the extracted stars and filter out the space targets in the image. Finally, based on the attitude of the satellite, camera parameters, and the coordinates of the target in the image, the precise pointing direction of the target can be calculated.

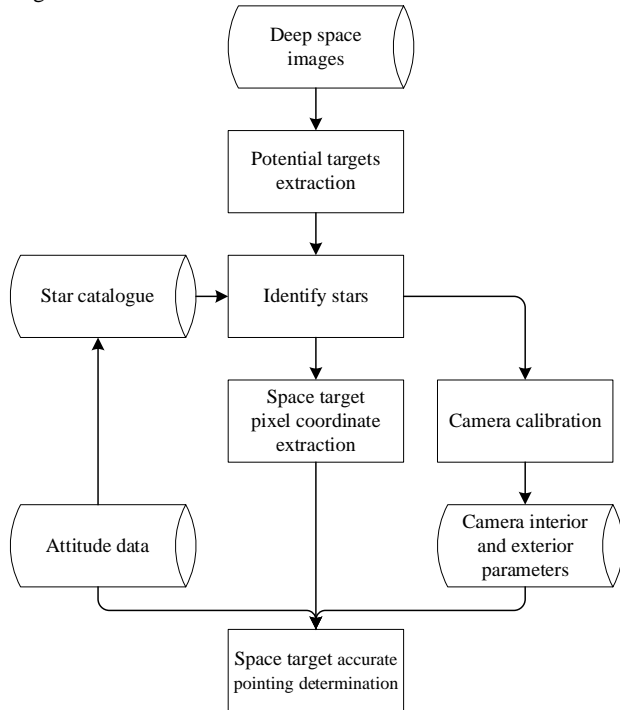


Figure 2. Processing flowchart of accurate pointing determination of space targets.

2.1 Potential Targets Extraction

When the camera photo the deep space, the background is black. But the camera has a certain background noise due to factors such as sensor current. It needs to be segmented by the threshold to separate the targets and the background in the image. Assuming that the digital number (DN) value of the image containing the space target is expressed as $g(x, y)$, and t is the background threshold, the image binarization is:

$$f(x, y) = \begin{cases} 1, & g(x, y) \geq t \\ 0, & g(x, y) < t \end{cases} \quad (1)$$

Since this experiment involves deep space photography at different orbital positions, the image will inevitably be affected by sunlight at some imaging angles. Therefore, the size and distribution of background noise vary, and thresholds can be set based on the mean and variance of the entire image.

The part of $f(x, y)$ with a value of 1 is marked by the connected domain algorithm, and k groups of connected domains $\Omega_i, i = \{1, 2, \dots, k\}$ are obtained. Each group of connected domains is

composed of different numbers and adjacent pixels, which can be expressed as follows:

$$\forall \Omega_i \in C \cap \forall \Omega_j \in C = 0, i \neq j, C = \{1, 2, \dots, k\}, \quad (2)$$

Each connected domain combination is a potential target (star or space target). If the attitude remains unchanged in the inertial frame during satellite imaging, the stars are shown as a round shape. By calculating the area and circularity of the connected domain, some brighter stars can be preliminarily filtered out. The round rate calculation formula is as follows (Guan, et al., 2022):

$$P = \frac{4\pi S}{L^2}, \quad (3)$$

among them, P represents the round rate, S represents the area of the connected domain, and L represents the perimeter of the connected domain. From the relationship between the circular area and the perimeter, it can be seen that the closer P is to 1, the more circular the connected domain is. Usually, the round rate of the star is greater than 0.6.

When the stars are filtered out, the centroid coordinates (x, y) of the star coordinates can be extracted by the grey square weighted centroid method. The calculation formula is:

$$\begin{cases} x = \sum_{(x,y) \in \Omega} x \cdot g(x, y)^2 / \sum_{(x,y) \in \Omega} g(x, y)^2 \\ y = \sum_{(x,y) \in \Omega} y \cdot g(x, y)^2 / \sum_{(x,y) \in \Omega} g(x, y)^2 \end{cases}, \quad (4)$$

2.2 Identify Stars

It is difficult to perform star identification directly based on the extracted stars. Because typical star identification requires a large number of bright stars in the field of view (usually brighter than 7th magnitude stars). However, the field of view of satellite cameras is small, and there may not be a bright star in image. But we can use satellite imaging models, combined with detailed star catalogues, to obtain the possible positions of stars in the image. Furthermore, distinguish between stars and non-star targets in the image. So, the geometric relationship between the image-side and the object-side is the key to this study.

According to the small hole imaging model, there should be a one-to-one correspondence between the star vector obtained by the camera and the star catalogue vector. The ascension and declination of the i -th star in the J2000 coordinate system are (α_i, δ_i) , which can be expressed as the azimuth vector Z_i :

$$Z_i = \begin{bmatrix} \cos \alpha_i \cos \delta_i \\ \sin \alpha_i \cos \delta_i \\ \sin \delta_i \end{bmatrix}, \quad (5)$$

When the i -th star is photographed, the attitude matrix of the camera in the J2000 coordinate system is R_{J2000}^{Cam} , then the relationship between the vector W_i (the i -th star in the camera coordinate system) and Z_i is:

$$W_i = R_{J2000}^{Cam} Z_i, \quad (6)$$

After imaging by the camera, the coordinates of the i -th star on the image are (x_i, y_i) , then the relationship between W_i and the coordinates of the image point is:

$$W_i = \begin{bmatrix} W_{i1} \\ W_{i2} \\ W_{i3} \end{bmatrix} = \frac{1}{\sqrt{((x_i - x_0)^2 + (y_i - y_0)^2 + f^2)}} \begin{bmatrix} x_i - x_0 \\ y_i - y_0 \\ -f \end{bmatrix}, \quad (7)$$

among them, f is the main distance of the optical lens of the camera, and (x_0, y_0) is the intersection of the optical axis of the camera and the image plane. According to the above formula, the calculation formula for the coordinates of the i -th star can be obtained as:

$$\begin{cases} x_i = x_0 - \frac{w_{i1}}{w_{i3}} * f \\ y_i = y_0 - \frac{w_{i2}}{w_{i3}} * f \end{cases} \quad (8)$$

Bring all the stars from the star catalogue into formula (5), (6), (7) and (8), then the stars which will be projected on the image are selected. Comparing the distance between the projected stars and the extracted targets. Within a certain threshold range, the pairing is considered as stars. And the corresponding relationship between the star coordinates in image and the right ascension/declination of stars in the J2000 system is established.

2.3 Camera Calibration

The above calculation process did not consider the error of camera's exterior and interior parameters. The accurate camera exterior parameters can be easily calculated based on the formula (6) (Guan et al., 2019). The interior distortion of camera can be divided into two types: radial distortion and tangential distortion. Usually, taking the first order of two kinds of distortion can well fit the lens distortion. Therefore, the distortion model is expressed as follows (Chen et al., 2022):

$$\begin{cases} \Delta x = k_1 x_a r_a^2 + p_1 (3x_a^2 + y_a^2) + 2p_2 x_a y_a \\ \Delta y = k_1 y_a r_a^2 + p_2 (3y_a^2 + x_a^2) + 2p_1 x_a y_a \end{cases} \quad (9)$$

where, $r_a = \sqrt{(x_a - x_0)^2 + (y_a - y_0)^2}$, k_1 represents first-order radial distortion, and p_1 and p_2 represent two parameters of first-order tangential distortion. The angular distance between any two stars, can be considered constant. So, for the star a and star b, the angle θ_{ab} between them is unchanged, and has the following relationship:

$$\cos\theta_{ab} = w_a^T w_b = (Mv_a)^T Mv_b = v_a^T M^T Mv_b = v_a^T v_b \quad (10)$$

According to the corresponding relation, the error model can be constructed for all the identified stars. The interior orientation parameters of camera to be estimated are:

$$X = [\Delta x_0 \quad \Delta y_0 \quad f \quad k_1 \quad p_1 \quad p_2] \quad (11)$$

The error model is as follows:

$$w_a^T w_b = \frac{x_a x_b + y_a y_b + f^2}{\sqrt{(x_a^2 + y_a^2 + f^2)(x_b^2 + y_b^2 + f^2)}} = G(X) \quad (12)$$

Where

$$\begin{cases} Xa = x_a - \Delta x_a, Xb = x_b - \Delta x_b \\ Ya = y_a - \Delta y_a, Yb = y_b - \Delta y_b \end{cases} \quad (13)$$

Take the partial derivative of the model and linearize it into:

$$V = \left[\frac{\partial G}{\partial \Delta x_0}, \frac{\partial G}{\partial \Delta y_0}, \frac{\partial G}{\partial f}, \frac{\partial G}{\partial k_1}, \frac{\partial G}{\partial p_1}, \frac{\partial G}{\partial p_2} \right] \Delta X - (\hat{v}_a^T \hat{v}_b - \hat{w}_a^T \hat{w}_b) \quad (14)$$

The least square iteration method can effectively estimate the above parameters, and after several iterations, the estimated value tends to be stable.

2.4 Space Target Pointing Determination

Based on all the targets extracted in the first step, excluding the stars extracted in the second step, potential space target coordinates are obtained. Suppose that the coordinates of the space target in the image plane coordinate system are (x_t, y_t) . The target pointing determination could be composed of the right ascension and declination (α, δ) as:

$$\begin{bmatrix} \cos\alpha \cdot \cos\delta \\ \sin\alpha \cdot \cos\delta \\ \sin\delta \end{bmatrix} = R_{Cam}^{J2000} \begin{bmatrix} x_t - \Delta x_0 \\ y_t - \Delta y_0 \\ -f \end{bmatrix} \quad (15)$$

On the right side of the formula (15) are all known quantities, including the attitude of the camera R_{Cam}^{J2000} and the interior parameters $(\Delta x_0, \Delta y_0, f)$ after camera calibration. The right ascension and declination (α, δ) information of space targets in the J2000 coordinate can be accurately obtained.

3 Data

In just one launch mission on Jun. 15th, 2023, more than 30 GF06A satellites were launched, making this series of satellites very suitable for tasks such as space target detection and monitoring. Figure 3 shows the satellite structure design diagram of Jilin-1 GF06A series. The GF06A series satellites can provide video and push-broom imaging, with a ground resolution of 0.75m and a satellite weight of only 22kg. Table 1 provides more detailed information on this series of satellites.



Figure 3. The satellite structure design diagram of Jilin-1 GF06A.

The data for this experiment comes from a deep space imaging mission of the GF06A-20 satellite on January 22nd, 2024. The imaging time for this task was 90 seconds. Each image was exposed for 10 seconds and a total of 9 images were captured.

The star catalogue data used in this experiment is the GAIA EDR2 catalogue data published in April 2018 by the European Space Agency (ESA) mission Gaia, which contains the measurement parameters of 1.69 billion celestial bodies. The original GAIA star catalogue contains the highest 21 magnitude stars, and the original data volume is about 1.26TB. Considering the processing time, this experiment selects stars with magnitude less than 16 in the GAIA catalogue as the pointing control point. The experimental star catalogue contains about 77319362 celestial bodies.

Overall	Launch Date	Jun. 15 th 2023
	Satellite numbers	30
Orbit parameters	Type	Sun synchronous
	Height	535km
	Frequency	1 Hz
Camera parameters	Image resolution	0.75m (panchromatic) 3m (multispectral)
	Imaging width	18km
	Focal length	1.6 m
	Field view	2°× 0.4°
CMOS parameters	CMOS numbers	2
	Pixel numbers	9344 (length) 3520 (width)
Attitude parameters	Triaxial error	X/Y: 7", Z: 30"
	Frequency	4 Hz

Table 1. The design parameters of Jilin-1 GF06A satellite.

4 Experimental Result and Analysis

In the following part of this study, we will provide a detailed result to the key parts used for accuracy pointing determination of space targets, namely star extraction, star identification and camera calibration.

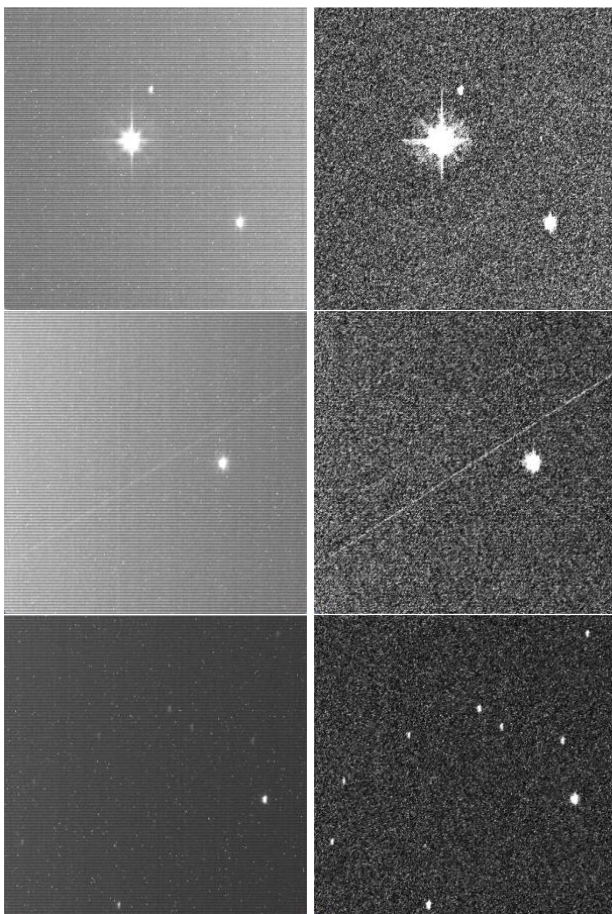


Figure 4. Original deep space images and background noise removal results.

There are many stars in the images captured in deep space. As shown in Figure 4, there are three typical sets of original deep space images and denoised images. These images are all captured

from a small portion within the complementary metal oxide semiconductor (CMOS) field of view. The first set of original images contains a brighter star. The second set of target motion trajectories and stars appear simultaneously. The third set of original images can extract numerous stars after denoising. Statistics were conducted on all stars within the field of view, and Figure 5 provides images of typical stars and their coordinate information in the image and object sides. From the brightest magnitude of 6.08 to the darkest magnitude of 15.62. As the magnitude increases, the area of stars in the image becomes smaller and harder to identify.

Mag=6.08 Sample=5353.64 Line=888.97 Lat=-8.81646° Lon=127.08251°	Mag=8.35 Sample=5139.14 Line=1637.67 Lat=-8.72953° Lon=127.05943°	Mag=9.30 Sample=7013.80 Line=3436.20 Lat=-8.52610° Lon=127.28243°
Mag=9.97 Sample=2593.52 Line=3133.80 Lat=-8.55061° Lon=126.76564°	Mag=11.02 Sample=6934.39 Line=2543.69 Lat=-8.62906° Lon=127.27106°	Mag=12.01 Sample=6895.98 Line=2964.42 Lat=-8.58035° Lon=127.26754°
Mag=13.01 Sample=7080.21 Line=45.61 Lat=-8.91779° Lon=127.28190°	Mag=14.50 Sample=4990.13 Line=3327.83 Lat=-8.53395° Lon=127.04612°	Mag=15.62 Sample=5314.13 Line=3311.30 Lat=-8.53658° Lon=127.08373°

Figure 5. Typical stars and their coordinate information.

In this deep space photography experiment, the attitude of the satellite in the inertial frame remains unchanged. So, within a 90 second imaging time, the stars within the field of view are basically the same for each CMOS. Each image is exposed for 10 seconds, so we can stack 9 images together. Figures 6 and 7 show the results taken by CMOS 1 and CMOS 2, respectively. The black origin is the position of the stars calculated through the star catalogue, and the larger it is, the brighter the stars (the smaller their magnitude). The red circle represents the stars identified in this study, with a maximum identified magnitude of 15.6. After the detection of this study, one space target was found in CMOS1, and four space targets were found in CMOS2. The red box in Figure 6 represents the position of the target in the 7 scenes. The number of times each space target appears in Figure 8 is different because they do not appear simultaneously. But the changes in these positions can reflect the motion of space targets in inertial coordinate.

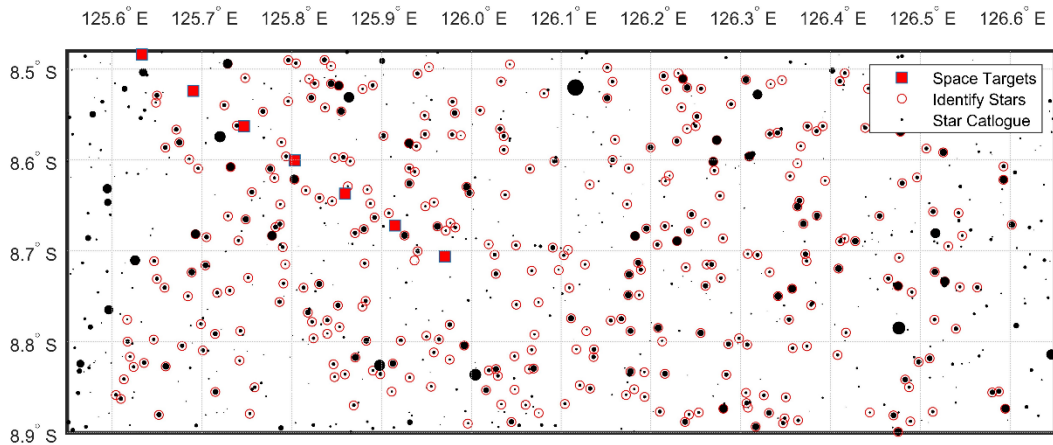


Figure 6. Star identification and space target extraction results of CMOS1 after stacking multiple images.

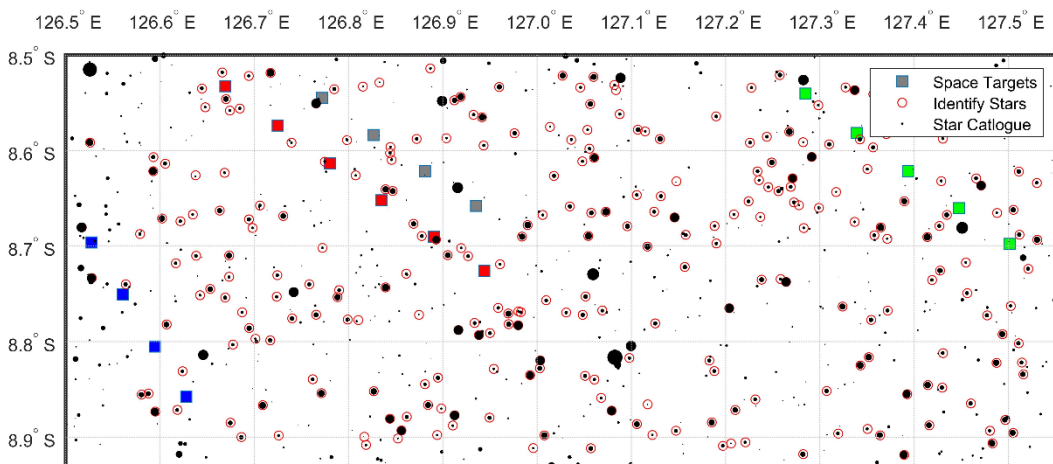


Figure 7. Star identification and space target extraction results of CMOS2 after stacking multiple images.

In a relatively short period of time (within a few years), the relative positions between the majority of stars in the sky are fixed. Therefore, the angular distance between two stars should be a fixed value and consistent with the calculated values in the star catalogue. Due to the orientation element error within the camera, there may be errors in the angular distance. Through these obtained stars, we can correct the camera's pointing. Due to the abundance of stars, we can even construct distortion models to obtain more accurate camera interior parameters. Before proceeding with the next step of space target extraction, it is necessary to perform the above two steps to achieve precise camera orientation. As shown in the Figure 8, the error of star diagonal distance before and after camera calibration. Before calibration, the root mean square error (RMSE) of the camera's star diagonal distance was 6.33 arcseconds, and after calibration, the RMSE was 0.48 arcseconds. Therefore, correcting the camera is a crucial step in determining the direction of space targets.

In this mission, due to long time exposure, a continuously moving target appeared in the field of view and formed a trajectory on the image. As shown in Figure 9. The left image is from the scene 4 of CMOS 2. S1 is the position of the space target at the beginning of the image exposure, and S2 is the position at the end of the image exposure. The white lines represent the motion trajectory of the space target during a 10 second exposure time. The image on the right is from the scene 5 of CMOS 2. After the previous scene ends exposure, the next scene starts exposure again. So, the starting exposure position S2 is exactly the same as the previous

scene, and the ending exposure position is S3. The corresponding relationship between stars in the two graphs also reveals the trajectory of continuous motion of space targets. Due to the long duration of the entire trajectory, within the 10 second exposure time range, we are unable to determine the corresponding time for the middle part of the trajectory. But we can know the time when the trajectory starts or end to appear in the image. Therefore, we can measure the image coordinates of the starting position of the space target trajectory in each scene. Then, using the camera geometry model, accurate space target pointing determination results are obtained.

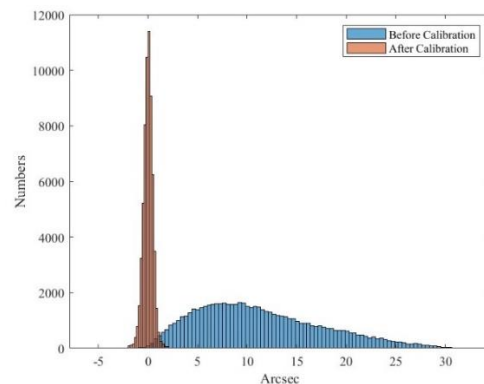


Figure 8. Star diagonal distance before and after calibration

Table 2 shows the cataloguing information for all space targets. The Target ID represents the number of the target. "Image belong" represents the source image of the measurement data, including two CMOS and the scene number. Date and time represent the observed coordinated universal time (UTC) of the target

appearance in the image. Pixel sample and line represents the coordinate information of the target in the image. The last two columns represent the coordinates of the target in the J2000 coordinate system.

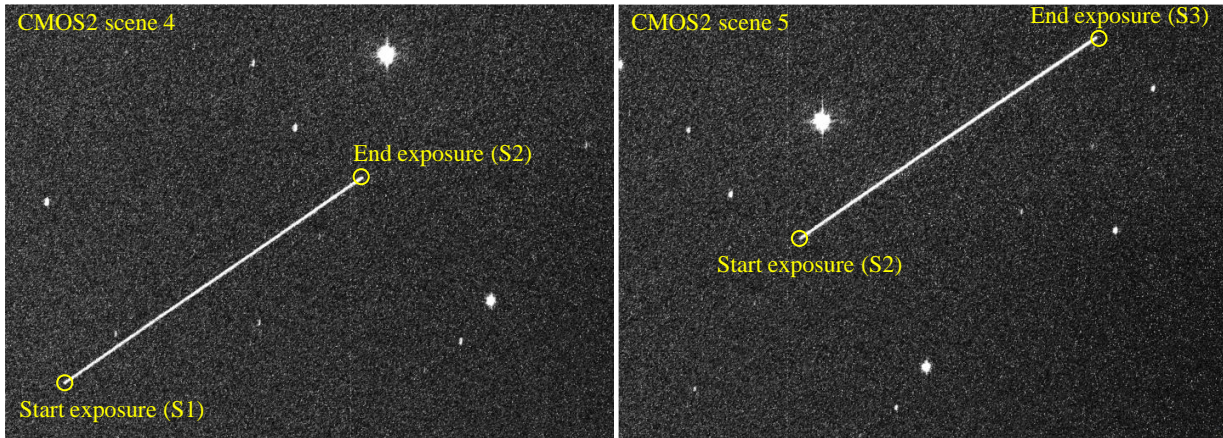


Figure 9. Schematic diagram of adjacent image space target motion and trajectory exposure

Table 2. The cataloguing information of space targets for Jilin-1 GF06A satellite.

Target ID	Images belong	Date	Time (UTC)	Pixel Sample	Pixel Line	J2000 Latitude/°	J2000 Longitude/°
001	CMOS1 scene 3	2024-01-22	00:48:51.0	535	3485	-8.48367	125.63300
	CMOS1 scene 4	2024-01-22	00:49:01.0	1032	3148	-8.52390	125.69021
	CMOS1 scene 5	2024-01-22	00:49:11.0	1525	2825	-8.56273	125.74676
	CMOS1 scene 6	2024-01-22	00:49:21.0	2015	2510	-8.60043	125.80314
	CMOS1 scene 7	2024-01-22	00:49:30.9	2503	2206	-8.63689	125.85929
	CMOS1 scene 8	2024-01-22	00:49:40.9	2985	1913	-8.67196	125.91483
002	CMOS2 scene 2	2024-01-22	00:48:40.99	1762	3272	-8.53252	126.66938
	CMOS2 scene 3	2024-01-22	00:48:50.98	2249	2927	-8.57384	126.72487
	CMOS2 scene 4	2024-01-22	00:49:00.97	2730	2592	-8.61357	126.78031
	CMOS2 scene 5	2024-01-22	00:49:10.96	3205	2269	-8.65211	126.83486
	CMOS2 scene 6	2024-01-22	00:49:20.96	3689	1946	-8.69049	126.89060
	CMOS2 scene 7	2024-01-22	00:49:30.95	4152	1648	-8.72597	126.94393
003	CMOS2 scene 2	2024-01-22	00:48:40.99	7033	3311	-8.54046	127.28475
	CMOS2 scene 3	2024-01-22	00:48:50.98	7509	2966	-8.58167	127.33904
	CMOS2 scene 4	2024-01-22	00:49:00.97	7982	2628	-8.62165	127.39362
	CMOS2 scene 5	2024-01-22	00:49:10.96	8451	2303	-8.66032	127.44753
004	CMOS2 scene 6	2024-01-22	00:49:20.96	8916	1986	-8.69788	127.50114
	CMOS2 scene 4	2024-01-22	00:49:00.97	581	1831	-8.69613	126.52752
	CMOS2 scene 5	2024-01-22	00:49:10.96	876	1365	-8.75077	126.56067
	CMOS2 scene 6	2024-01-22	00:49:20.96	1176	900	-8.80512	126.59455
005	CMOS2 scene 7	2024-01-22	00:49:30.95	1472	451	-8.85765	126.62797
	CMOS2 scene 4	2024-01-22	00:49:00.97	2645	3184	-8.54503	126.77184
	CMOS2 scene 5	2024-01-22	00:49:10.96	3121	2859	-8.58380	126.82649
	CMOS2 scene 6	2024-01-22	00:49:20.96	3596	2541	-8.62158	126.88118
	CMOS2 scene 7	2024-01-22	00:49:30.95	4067	2236	-8.65788	126.93541

By comparing the target grayscale value with the star grayscale value, it can be found that the grayscale value of the target is close to that of a 15-magnitude star. This is a very low brightness value, indicating that this series of satellites has great potential in space target detection. In the subsequent detection tasks, the exposure time of each scene will be reduced to obtain more target pointing information at different time. In this way, the movement pattern of the target can be calculated based on the position of the satellite, the direction of the target, and orbital dynamics.

5 Conclusion

This study proposes a method for pointing determination of space targets through satellite observation on deep space. The focus of this method is to extract the stars and use them to calibrate the camera. Finally, the high precision pointing of the space target can be calculated and cataloguing.

Acknowledgements

This work was supported by the National Natural Science Foundation of China (42301424) and Key Research and Development Program Plan of Hubei Province (2021BLB152). This work has made use of data from the ESA mission Gaia (<https://www.cosmos.esa.int/gaia>), processed by the Gaia Data Processing and Analysis Consortium DPAC, (<https://www.cosmos.esa.int/web/gaia/dpac/consortium>). Funding for the DPAC has been provided by national institutions, in particular the institutions participating in the Gaia Multilateral Agreement.

References

- Chen X, Xing F, You Z, Zhong X, Qi K, On-Orbit High-Accuracy Geometric Calibration for Remote Sensing Camera Based on Star Sources Observation. *IEEE Transactions on Geoscience and Remote Sensing*, 1-11, 2022.
- Gruntman, M., 2014. Passive optical detection of submillimeter and millimeter size space debris in low Earth orbit. *Acta Astronautica*, 105(1): 156-170.
- Guan Z, Jiang Y, Wang J, Zhang G. Star-Based Calibration of the Installation Between the Camera and Star Sensor of the LuoJia 1-01 Satellite. *Remote Sensing*.11(18):2081, 2019.
- Guan, Z., Zhang, G., Jiang, Y., Zhong, X., Deng, M., Li, B., and Zhang, H.: Detection of the Angle Change Between Camera and Star Tracker Base on Star Observation, *ISPRS Ann. Photogramm. Remote Sens. Spatial Inf. Sci.*, V-1, 77–83, 2022. <https://doi.org/10.5194/isprs-annals-V-1-2022-77-2022>
- Guan, Z., Zhang, G., Jiang, Y., Shen X.: Low-Frequency Attitude Error Compensation for the Jilin-1 Satellite Based on Star Observation, *IEEE Transactions on Geoscience and Remote Sensing*, 61, 1-17, 2023.
- Liu, M., Wang H., Yi, H., Xue, Y., Wen, D., Wang, F., Shen, Y., Pan, Y. 2022. Space Debris Detection and Positioning Technology Based on Multiple Star Trackers. *Applied Sciences*, 12(7): 3593.
- Lupo, R., Albanese, C., Bettinelli, D., Brancati, M., Minei, G., Pernechele, C. 2018. Lighthouse: A spacebased mission concept for the surveillance of geosynchronous space debris from low earth orbit. *Advances in Space Research*, 62(12): 3305-3317.
- Samadzadegan, F. and Alidoost, F., 2013. The Design and Implementation of an Optical Astronomical Satellite Tracking System. *Int. Arch. Photogramm. Remote Sens. Spatial Inf. Sci.*, XL-1/W3: 25-30. <https://doi.org/10.5194/isprsarchives-XL-1-W3-25-2013>